Stellar Migration and Chemical Enrichment in the Milky Way Disc: On the Nucleosynthesis of Nitrogen

James W. Johnson,[1]★ David H. Weinberg,[1,2,3] Fiorenzo Vincenzo,[1,2] Jonathan C. Bird,[4] and Emily J. Griffith[1]

[1] *Department of Astronomy, The Ohio State University, 140 W. 18th Ave., Columbus, OH, 43210, USA*
[2] *Center for Cosmology and Astroparticle Physics (CCAPP), The Ohio State University, 191 W. Woodruff Ave., Columbus, OH, 43210, USA*
[3] *Institute for Advanced Study, 1 Einstein Dr., Princeton, NJ, 08540, USA*
[4] *Department of Physics & Astronomy, Vanderbilt University, 2301 Vanderbilt Place, Nashville, TN, 37235, USA*

Accepted XXX; Received YYY; in original form ZZZ

ABSTRACT

We use a multi-ring galactic chemical evolution model to probe the astrophysical production of nitrogen (N) in the Milky Way. This approach treats individual annuli in the Galaxy disc as a conventional one-zone model, and to include the effects of radial migration, stellar populations move between annuli in a manner informed by a hydrodynamical simulation. We test how well different AGB star nucleosynthetic yield models for N can reproduce the observed [N/O]-[O/H] relation. We find that no published set of AGB star yields is able to reproduce the data; those that reproduce the qualitative trend still require an artificial enhancement of their N yields by factors of a few. We find that N production timescales are sufficiently short such that stellar migration is only a minimal source of intrinsic scatter in the observed [N/O]-[O/H] relation. Typical variations in the star formation rate and star formation efficiency produce considerably larger variations in the gas phase N and O abundances, consistent with previous observational arguments. We demonstrate that when a viable AGB star yield table is adopted, our model is able to reproduce many of the observed correlations between N, O, and Fe abundances for stars when the N abundances are corrected for internal mixing processes. Our models run using the publicly available `Versatile Integrator for Chemical Evolution` (`VICE`; https://pypi.org/project/vice).

Key words: Awesomeness

1 INTRODUCTION

• Nitrogen (N) is an element that traces slow neutron capture (s-process) nucleosynthesis. To first order it's produced only in core collapse supernovae (CCSNe) and asymptotic giant branch (AGB) stars (Johnson 2019).

• The observed [N/O]-[O/H] relation in the gas phase is more or less the same between different environments. We demonstrate this in Fig. 1 where we compile measurements from previous studies interested in various astrophysical systems.

• Qualitatively, the rise in N abundances with increasing [O/H] can be attributed to the metallicity-dependent nature of N yields from AGB stars (Vincenzo et al. 2016; see also discussion in § X).

• How well do chemical evolution models for the Milky Way with various "off-the-shelf" yield models perform at reproducing this trend?

• Nitrogen has considerable yields through *secondary* channels: the processing of already produced metals into nitrogen.

– First and foremost is the CNO cycle, in which carbon (C), N, and oxygen (O) catalyze the fusion of four protons into helium-4. The reactions of the CNO cycle:

$$^{12}\mathrm{C}(p,\gamma)^{13}\mathrm{N}(\beta^+,\nu_e)^{13}\mathrm{C}(p,\gamma)^{14}\mathrm{N}(p,\gamma)^{15}\mathrm{O}(\beta^+,\nu_e)^{15}\mathrm{N}(p,\alpha)^{12}\mathrm{C} \quad (1)$$

Due to a small cross section for proton capture, the $^{14}\mathrm{N}(p,\gamma)^{15}\mathrm{O}$ reaction is particularly slow. As a result, to first order the effect of the CNO cycle is to process all of the available C and O into ^{14}N.

• Fig. 1 presents a compilation of observed abundances of N and O in the gas phase:

– HII regions in nearby NGC spirals (Pilyugin et al. 2010)
– HII regions in blue, diffuse star forming dwarf galaxies (Berg et al. 2012; Izotov et al. 2012; James et al. 2015)
– Local stars and HII regions (Dopita et al. 2016)
– Galactic and extragalactic HII regions (Henry et al. 2000)
– Star-forming regions in 550 nearby galaxies in the MaNGA IFU survey (Belfiore et al. 2017)

Despite intrinsic scatter and some systematic variation in how the abundances are determined, the [N/O]-[O/H] relation is more or less the same across a wide range of physical enrivonments.

• In this paper, we're interested in the origin of both the shape and scatter in this trend.

• In a sample of 6,507 galaxies from the Mapping Galaxies at Apache Point Observatory survey (MaNGA; Bundy et al. 2015), Schaefer et al. (2020) recently argued that intrinsic scatter in the [N/O]-[O/H] relation near and above solar metallicity is a consequence of variations in the local star formation efficiency. In regions of slower star formation, the [N/O] ratio tends to be slightly higher at fixed [O/H] (see their Fig. 4), as expected from chemical evolution models (e.g. Mollá et al. 2006; Vincenzo et al. 2016).

★ Contanct e-mail: johnson.7419@osu.edu

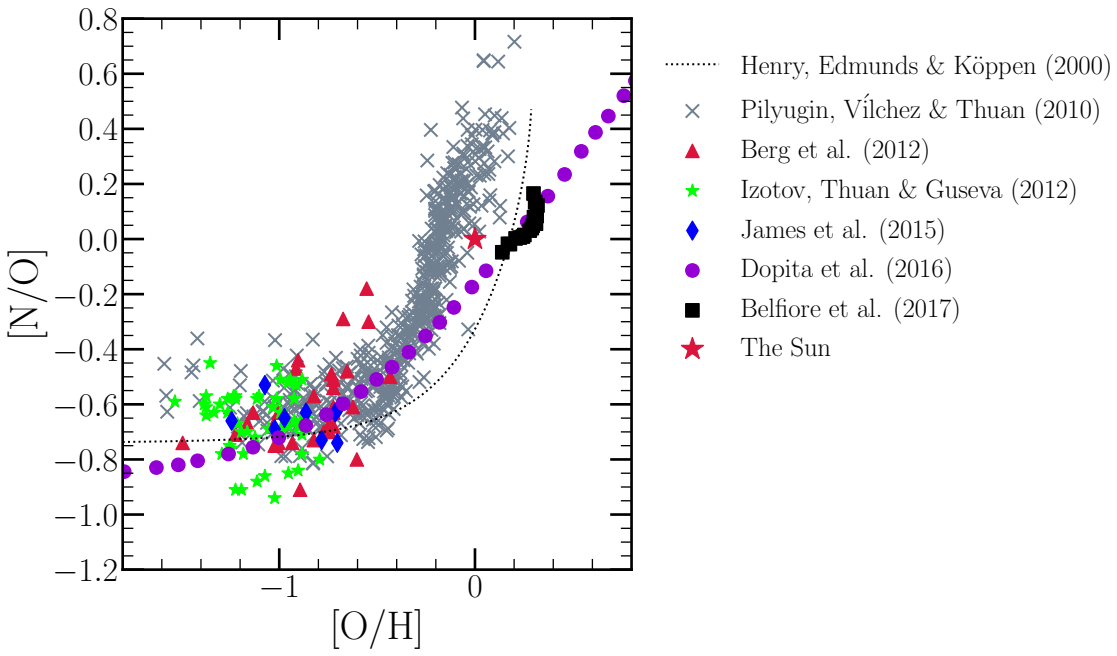

Figure 1. The [N/O]-[O/H] relation observed in HII regions in nearby NGC spiral galaxies (grey X's: Pilyugin, Vílchez & Thuan 2010), in HII regions in blue, diffuse star forming dwarf galaxies (red triangles: Berg et al. 2012; green stars: Izotov, Thuan & Guseva 2012; blue diamonds: James et al. 2015), in local stars and HII regions (purple circles: Dopita et al. 2016), and in the MaNGA IFU survey (black squares: Belfiore et al. 2017). The fit to [N/O] as a function of [O/H] in Galactic and extragalactic HII regions by Henry, Edmunds & Köppen (2000) is shown in a black dotted line. The Sun, at (0, 0) on this plot by definition, is marked by a red star. We omit the uncertainties for visual clarity.

2 METHODS

• Since we wish to test the impact of various assumptions about nucleosynthetic yields while taking into account stellar migration, multi-zone chemical evolution models are the ideal experiments.

2.1 The Multi-Zone Chemical Evolution Model

• We make use of the Milky Way models of Johnson et al. (2021), who originally constructed the model to explore the impact of stellar migration on the observed abundances of oxygen and iron. This model makes use of the `Versatile Integrator for Chemical Evolution` (`VICE`; Johnson & Weinberg 2020; Griffith et al. 2021; Johnson et al. 2021), an open-source `python` package for `Unix` system architectures. Because `VICE` recognizes most elements on the periodic table, computing N abundances with this model is easy. Though we provide a brief summary here, a full breakdown of the Johnson et al. (2021) model can be found in their § 2.

2.2 Nucleosynthetic Yields

• Since we're interested in N and O abundances in the present paper, the relevant nucleosynthetic channels are CCSNe and AGB stars (Johnson 2019). Johnson et al. (2021) investigated the O and Fe abundances predicted by these models, the relevant sources for which are CCSNe and SNe Ia. Here we simply set the SN Ia yields of N and O to zero, and focus the rest of this section on discussion of their CCSN and AGB star yields.

2.2.1 *Core Collapse Supernovae*

• For O and Fe, we retain the values of $y_{\rm O}^{\rm CC} = 0.015$ and $y_{\rm Fe}^{\rm CC} = 0.0012$ from Johnson et al. (2021), who in turn take these values from Johnson & Weinberg (2020) and Weinberg et al. (2017). In `VICE`, CCSN nucleosynthetic products are approximated to be produced instantaneously following an episode of star formation; this is a valid approximation due to how short the lives of massive stars are compared to the relevant timescales for GCE. The yield is the constant of proportionality between the CCSN production rate and the SFR:

$$\dot{M}_{\rm X}^{\rm CC} = y_{\rm X}^{\rm CC}\dot{M}_{\star}. \tag{2}$$

As a consequence of this formulation $y_{\rm X}^{\rm CC}$ describes the fraction of a stellar population's initial mass which is processed into some element X and ejected to the ISM via CCSN events (e.g. if $y_{\rm X}^{\rm CC} = 0.01$, a hypothetical 100 $M_\odot$ stellar population would produce 1 $M_\odot$ of element X).

• At low [O/H][1], the mean [N/O] is near ∼-0.7. Since the AGB star yields of N are believed to increase with metallicity (Cristallo et al. 2011, 2015; Ventura et al. 2013), this is likely the regime in which N yields are dominated by CCSN enrichment. Therefore, $[{\rm N/O}]_{\rm cc} \approx -0.7$ empirically.

• Based on the definition of the abundance ratio [X/Y], we can relate the CCSN yields of N and O to one another given this result:

$$[{\rm N/O}]_{\rm cc} = \log_{10}\left(\frac{y_{\rm N}^{\rm CC}}{y_{\rm O}^{\rm CC}}\right) - \log_{10}\left(\frac{Z_{\rm N,\odot}}{Z_{\rm O,\odot}}\right) \tag{3a}$$

$$y_{\rm N}^{\rm CC} = y_{\rm O}^{\rm CC} 10^{[{\rm N/O}]_{\rm cc}}\left(\frac{Z_{\rm N,\odot}}{Z_{\rm O,\odot}}\right), \tag{3b}$$

where $Z_{\rm X,\odot}$ is the abundance by mass of some element X in the sun.

• Taking $Z_{\rm N,\odot} = 6.91\times10^{-4}$ and $Z_{\rm O,\odot} = 5.7\times10^{-3}$ based on the solar photospheric abundances of Asplund et al. (2009) and our value of $y_{\rm O}^{\rm CC} = 0.015$ yields $y_{\rm N}^{\rm CC} = 3.6\times10^{-4}$, which we adopt as our fiducial CCSN yield of N.

• Can we understand this value with theoretically predicted N yields? To address this, we compute IMF-averaged net yields of N using `VICE`'s `vice.yields.ccsne.fractional` function assuming a Kroupa (2001) IMF; for details, we refer readers to § 4 of Griffith et al. (2021) and the `VICE` science documentation.[2] The left panel of Fig. 2 plots the results as a function of progenitor metallicity predicted

[1] We follow the standard notation where $[{\rm X/Y}] \equiv \log_{10}(X/Y) - \log_{10}(X/Y)_\odot$.
[2] https://vice-astro.readthedocs.io/en/latest/science_documentation/yields/index.html

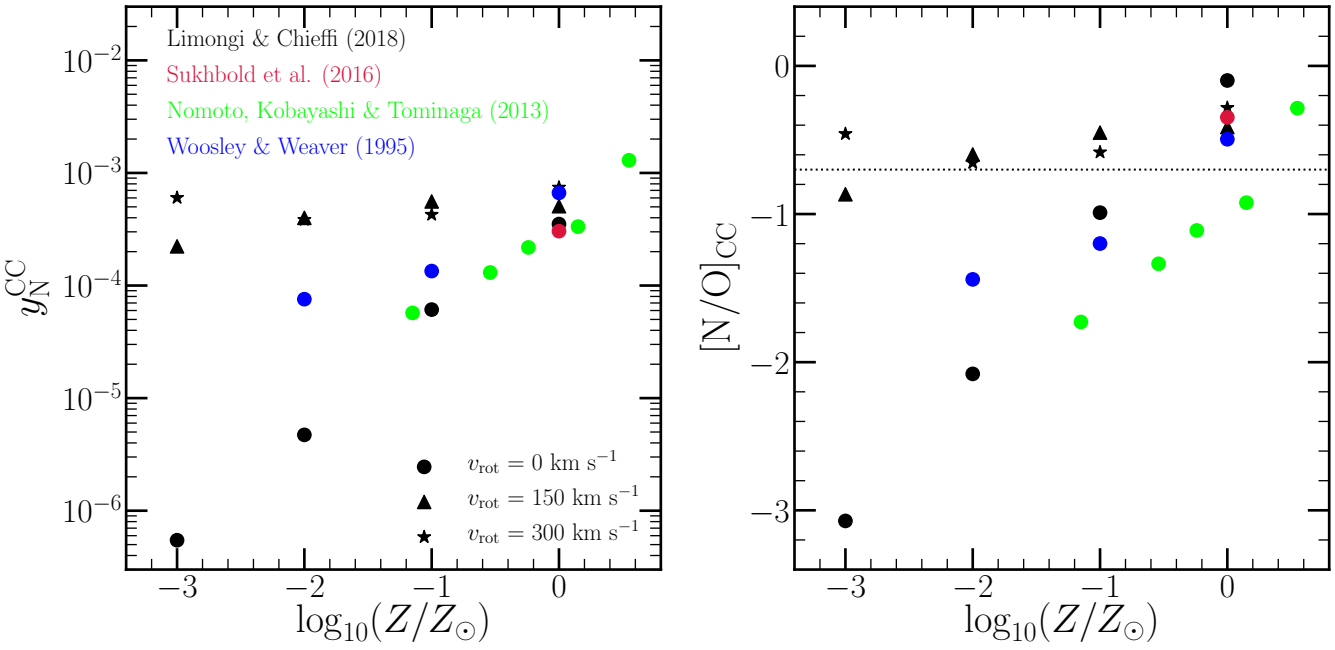

Figure 2. Left: IMF-averaged CCSN yields of N calculated using `VICE`'s `vice.yields.ccsne.fractional` function with the tables published by Woosley & Weaver (1995, blue), Nomoto, Kobayashi & Tominaga (2013, green), Sukhbold et al. (2016, red), and Limongi & Chieffi (2018, black). All studies report yields for non-rotating progenitors only with the exception of Limongi & Chieffi (2018), who also report yields for progenitor rotational velocities of 150 (triangles) and 300 km/s (stars). **Right**: The [N/O] ratio predicted by each of the explosion models in the left-hand panel, under the same colour-coding and marker scheme. We mark the position of [N/O] = −0.7 with a black dotted line, the value roughly suggested by the observations of low-metallicity systems highlighted in Fig. 1.

by the Woosley & Weaver (1995), Nomoto et al. (2013), Sukhbold et al. (2016), and Limongi & Chieffi (2018) tables.

- Only Limongi & Chieffi (2018) report yields for progenitors with a non-zero rotational velocity, and these are the only values consistent with $y_{\rm N}^{\rm CC} = 3.6 \times 10^{-4}$ at low metallicity. For non-rotating progenitors, every study investigated here can reproduce approximately this value at solar metallicity only, with the predictions at lower Z falling short of the empirical value, in some cases by orders of magnitude.
- It is unsurprising that $y_{\rm N}^{\rm CC}$ is so dependent on the rotational velocity at low metallicity. $y_{\rm N}^{\rm CC}$ is itself highly uncertain at low Z (Heger & Woosley 2010), but most of the N production in CCSN progenitors occurs via the CNO cycle processing C and O isotopes into ^{14}N. With few C and O seed nuclei at low Z, production of ^{14}N is difficult. Rotationally induced mixing, also a highly uncertain process (Frischknecht et al. 2016), could transport newly produced C and O into the hydrogen burning shell of the CCSN progenitor (see discussion in § 4.2 of Andrews et al. 2017). For this reason, N yields at low metallicity are highly sensitive to the assumptions about mixing.
- In the right-hand panel of Fig. 2, we make use of equation (3a) to compare the [N/O] ratios predicted by these studies; the horizontal black dashed line denotes $[{\rm N/O}]_{\rm cc} = -0.07$, the empirical value taken from Fig. 1. The fact that the points follow similar trends between the two panels is a consequence of the fact that these studies predict metallicity-independent O yields (Griffith et al. 2021).
- Again, only the rotating models of Limongi & Chieffi (2018) are able to reproduce this value at low metallicity. At solar metallicity the supernova models predict a higher $[{\rm N/O}]_{\rm cc}$, but our value of $[{\rm N/O}]_{\rm cc}$ is taken at low metallicity, so that is the most relevant comparison.

2.2.2 *Asymptotic Giant Branch Stars*

- In the present paper, we're interested in the question of how well the "off the shelf" AGB star yield models for N can reproduce the observed [N/O]-[O/H] relation.
- As previously discussed, the majority of nitrogen production occurs through the CNO cycle, the slowest component of which is the ^{14}N(p,γ)^{15}Oreaction which produces a bottleneck, effectively turning all of the different C, N, and O isotopes into ^{14}N.
- Similar to the CCSN yields discussed in § 2.2.1, these are defined as fractional net yields in that they quantify only the newly produced N in the AGB star ejecta in units of its ZAMS mass. For a yield $y_{\rm N}^{\rm AGB}(M_\star, Z_\star)$, the actual mass yield is then given by $M_\star y_{\rm N}^{\rm AGB}(M_\star, Z_\star)$.
- We make use of tables that are built into `VICE`, two of which are new to this study and are included in its latest release.
  - The default set of yields, published in Cristallo et al. (2011, 2015) is plotted in the lower left panel of Fig. 3. This is the most comprehensive set of yields in `VICE` in that it includes tables for all elements built into the code and is sampled at the most metallicities.
  - The Karakas (2010) set of yields, also previously built into `VICE`, is plotted in the upper left panel.
  - We obtain the yields from Ventura et al. (2013), which are new to `VICE`, and plot them in the lower middle panel.
  - We combine the yields published in Karakas & Lugaro (2016) at Z = 0.007, 0.014, and 0.03 with those published in Karakas et al. (2018) at Z = 0.0028 and build them into `VICE` as well. Although there are yields published in both Karakas & Lugaro (2016) and Karakas et al. (2018) in this table, we hereafter refer to this set as the Karakas & Lugaro (2016) set for simplicity. We plot them in the upper middle panel of Fig. 3.
- `VICE` also allows users to construct their own functions of progenitor mass and metallicity to describe the AGB star yield. As an additional test, we construct a model in which the yield is linearly proportional to both of them according to:

$$y_{\rm N}^{\rm AGB} = \xi \left(\frac{M}{M_\odot}\right)\left(\frac{Z}{Z_\odot}\right) \tag{4}$$

We illustrate this model in the lower right panel of Fig. 3 for $\xi = 3 \times 10^{-4}$. We compare this model to the Cristallo et al. (2011, 2015) yields by including the colored X's on this panel. In general, the two yield models agree rather well.

- Despite reporting values of the same physical quantities, the N yields reported by each of these studies show substantial differences between one another. Unfortunately, a direct comparison between AGB star yield tables is difficult, because each study employs different assumptions for mass loss, convection and covective boundaries

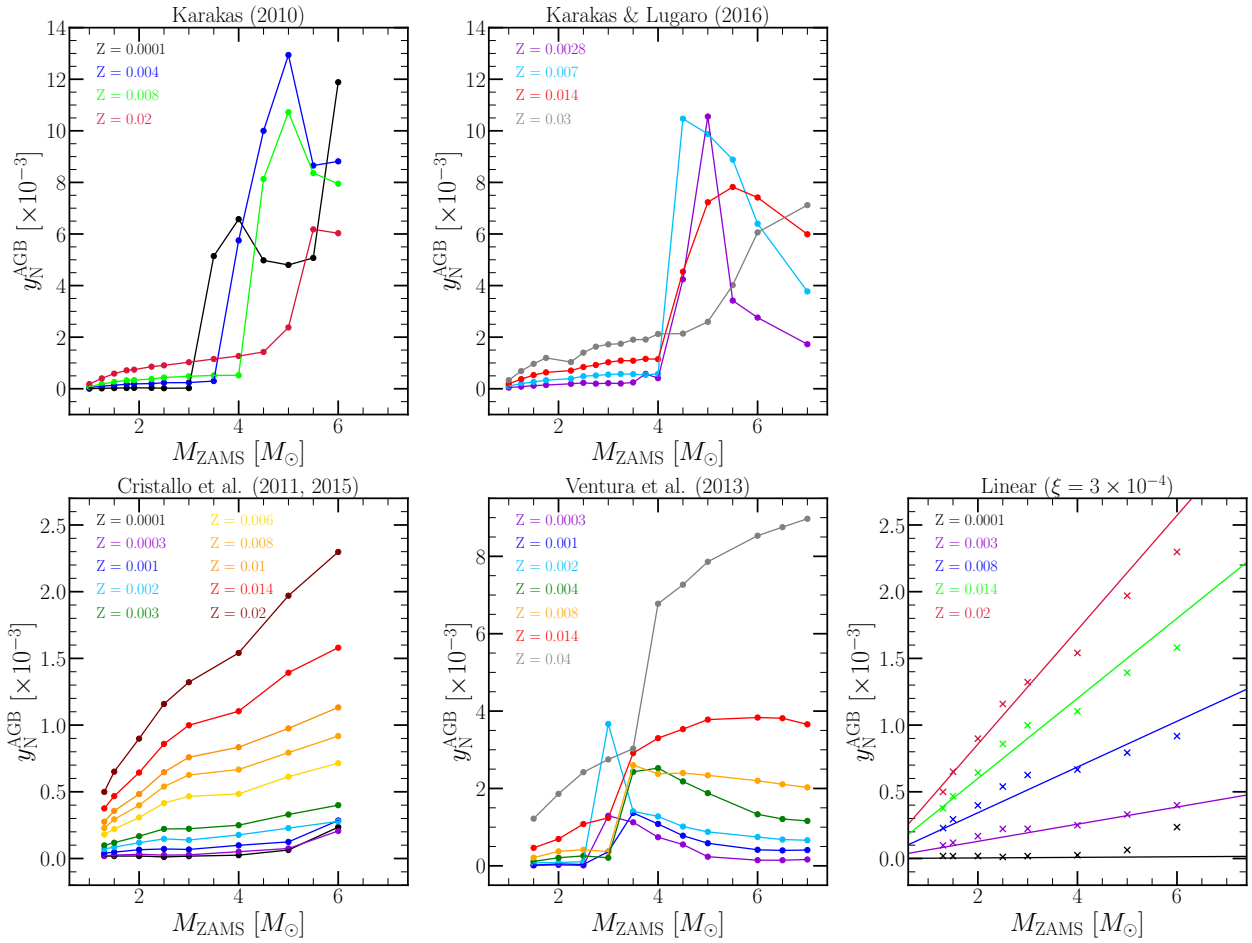

Figure 3. The fractional yields of N from AGB stars y_N^{AGB} as a function of progenitor ZAMS mass and birth metallicity Z as reported by Karakas (2010) (upper left), Karakas & Lugaro (2016) and Karakas et al. (2018) (upper middle), Cristallo et al. (2011, 2015) (lower left), and Ventura et al. (2013) (lower middle). In the lower right panel, we show the yields predicted by our linear model (colored lines; see discussion in § X) in comparison to the Cristallo et al. (2011, 2015) predictions (colored X's).

within the star, and nuclear reaction networks, all of which have a significant impact on stellar evolution and consequently the predicted abundances. However, the two most important physical processes in determining AGB star yields of all the CNO species is third dredge up (TDU) and hot bottom burning (HBB), and some of the differences between these yield sets can be understood through the interaction between the two.

– TDU refers to the repeated penetrations of the convective envelope into the hydrogen depleted core during the thermal pulses associated with AGB star evolution. This process doesn't affect N abundances much, but replenishes the outer layers of the star with C and O. In low mass AGB stars, the main source of free neutrons is the ^{13}C(α,n)^{16}O reaction, which can occur at substantial rates when C is mixed with the He-rich shell during each TDU episode.

– HBB refers to the activation of proton captures at the base of the convective envelope, which activates the CNO cycle, producing large amounts of ^{14}N. HBB requires a higher mass AGB star progenitor (~4 - 5 M$_\odot$at Z$_\odot$) than TDU (~2 - 2.5 M$_\odot$at Z$_\odot$), but the minimum mass for both decreases at lower metallicity.

– The most efficient N production occurs when both TDU and HBB occur within an AGB star, because each replenishment of C and O isotopes from the core adds new seed nuclei for the CNO cycle when HBB is active. This is the reason for the substantial N production above ~4 M$_\odot$in the Karakas (2010) and Karakas & Lugaro (2016) models; in both yield sets, every star that experiences HBB also experiences TDU. Both TDU and HBB are more efficient at low metallicity (see discussion in Ventura et al. 2013). In the case of TDU, each penetration of the convective envelope into the H-depleted core is deeper because of the lower opacity. For HBB, the base of the convective envelope is hotter, increasing the rate of nuclear reactions relative to the higher Z models. Though some exceptions are evident in Fig. 3, as a result of this the highest N yields in the Karakas (2010) and Karakas & Lugaro (2016) tables are for the low metallicity stars above ~4 M$_\odot$.

– This same interaction between TDU and HBB is also the reason for the increase in yields in the Ventura et al. (2013) sample. Unlike Karakas (2010) and Karakas & Lugaro (2016), their models experience both TDU and HBB only near ~3 M$_\odot$.

– Of all of these yields taken from the literature, the Cristallo et al. (2011, 2015) sample shows the smoothest dependence on progenitor mass and metallicity. Unfortunately, ascertaining the exact cause of this difference between the other yields explored here is difficult; relative to the Karakas & Lugaro (2016) yields (see discussion in their § 5), the Cristallo et al. (2011, 2015) models have more mass loss, a ~10% faster triple-α reaction rate, weaker HBB, and fewer thermal pulses overall. The fact that HBB is weaker and fewer TDU episodes are experienced does however lend a qualitative explanation into why the Cristallo et al. (2011, 2015) yields are so much smaller than the Karakas (2010) and Karakas & Lugaro (2016) yields at higher masses.

3 RESULTS

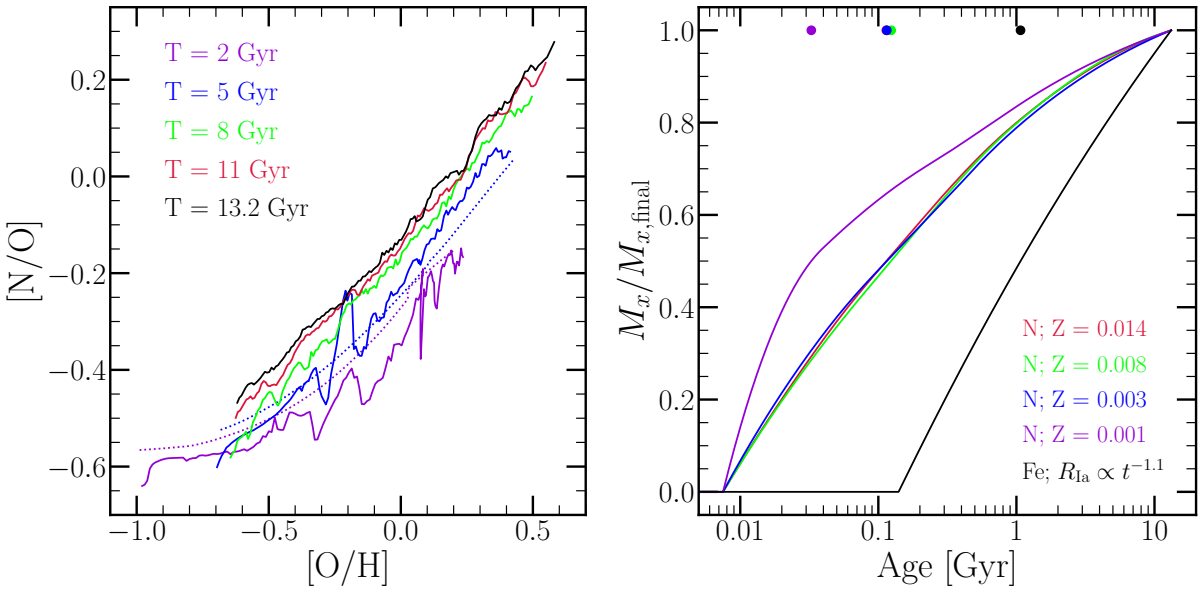

Figure 4. **Left**: The time evolution of the gas-phase [N/O]-[O/H] relation in our fiducial model with the C11+C15 yields (solid colored lines). Dotted lines denote the resulting relation when stellar migration is neglected at T = 2 and 5 Gyr. **Right**: The net mass of N produced by AGB stars from a single stellar population assuming four initial metallicities and the C11+C15 yields (colored lines). The black line denotes the same for Fe assuming the $t^{-1.1}$ power-law delay time distribution adopted in our models. All values are normalized to the total mass produced at an age of 13.2 Gyr. Points at the top of the panel denote the ages at which 50% of the total mass has been produced.

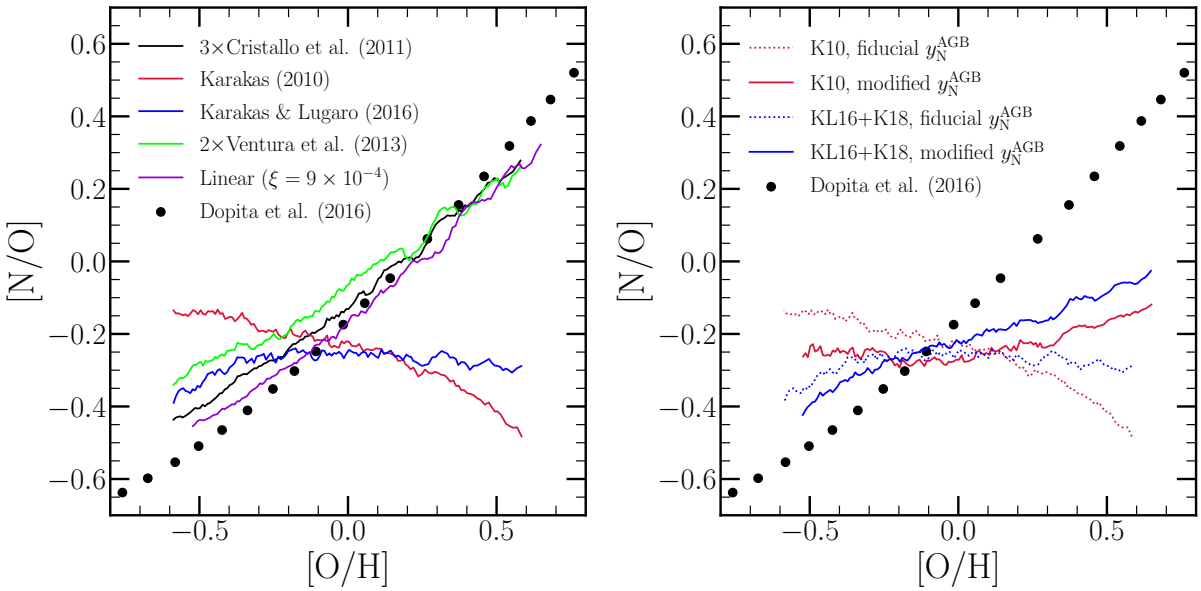

Figure 5. **Left**: The present day gas-phase [N/O]-[O/H] relation predicted by our fiducial model with each of the yield sets described in § 2.2.2. For observational reference, we plot the population-averaged trend for local stars and HII regions reported by Dopita et al. (2016). **Right**: The same as the left-hand panel, but comparing the predictions made by the K10 and KL16+K18 yields with our fiducial value of $y_{\mathrm{N}}^{\mathrm{CC}}$ (dotted lines, same as left-hand panel) to those with the alternate forms of $y_{\mathrm{N}}^{\mathrm{CC}}$ (solid lines) given by equation X for the K10 yields and equation Y for the KL16+K18 yields.

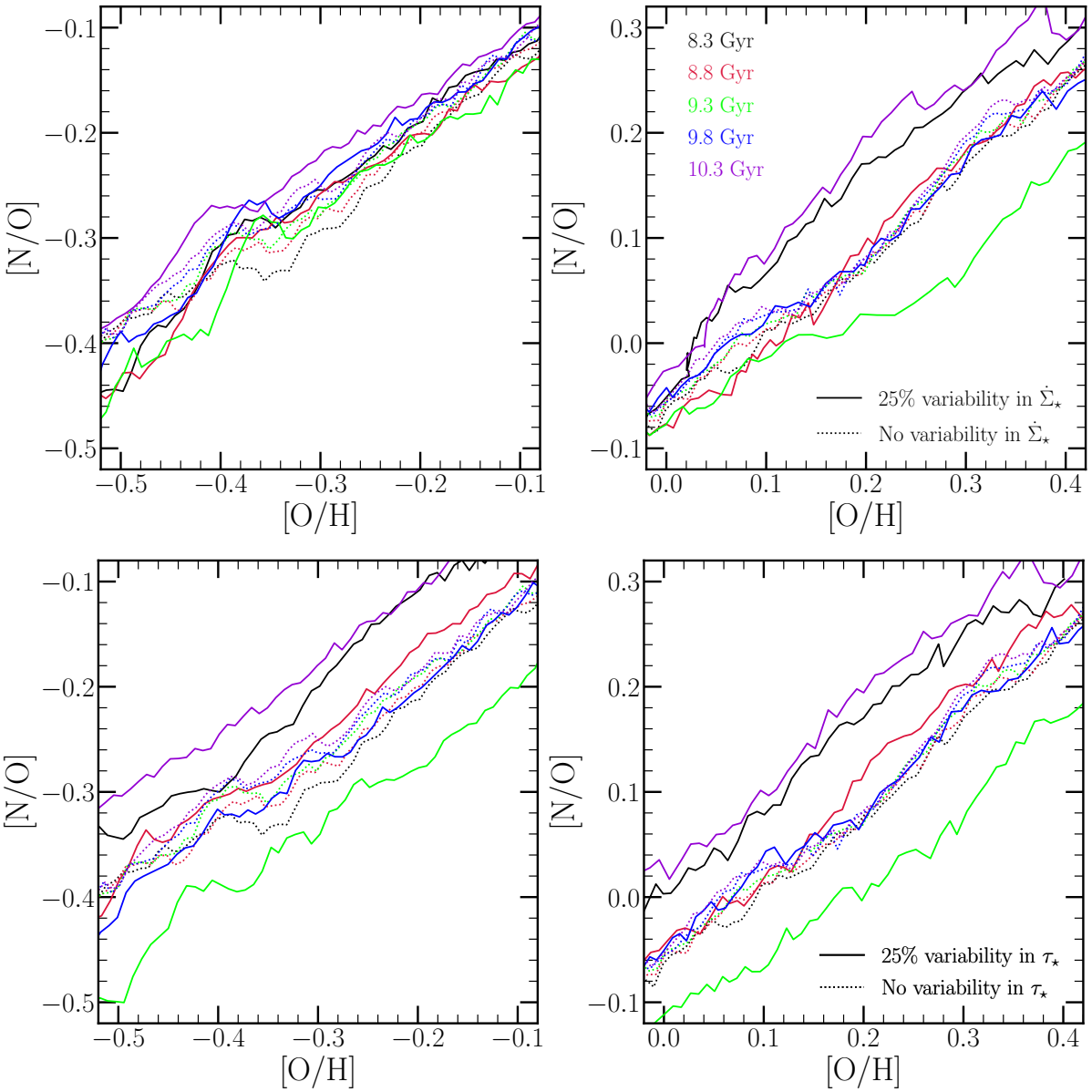

Figure 6. One cycle of variability in the gas-phase [N/O]-[O/H] relation at low [O/H] (left) and high [O/H] (right) induced by 25% sinusoidal variations in the SFR (top) and in the SFE (bottom). Solid lines denote the models with some source of variability, and dotted lines denote the fiducial model with no variability; all models take into account the effects of stellar migration.

REFERENCES

Andrews B. H., Weinberg D. H., Schönrich R., Johnson J. A., 2017, ApJ, 835, 224

Asplund M., Grevesse N., Sauval A. J., Scott P., 2009, ARA&A, 47, 481

Belfiore F., et al., 2017, MNRAS, 469, 151

Berg D. A., et al., 2012, ApJ, 754, 98

Bundy K., et al., 2015, ApJ, 798, 7

Cristallo S., et al., 2011, ApJS, 197, 17

Cristallo S., Straniero O., Piersanti L., Gobrecht D., 2015, ApJS, 219, 40

Dopita M. A., Kewley L. J., Sutherland R. S., Nicholls D. C., 2016, Ap&SS, 361, 61

Frischknecht U., et al., 2016, MNRAS, 456, 1803

Griffith E. J., Sukhbold T., Weinberg D. H., Johnson J. A., Johnson J. W., Vincenzo F., 2021, arXiv e-prints, p. arXiv:2103.09837

Heger A., Woosley S. E., 2010, ApJ, 724, 341

Henry R. B. C., Edmunds M. G., Köppen J., 2000, ApJ, 541, 660

Izotov Y. I., Thuan T. X., Guseva N. G., 2012, A&A, 546, A122

James B. L., Koposov S., Stark D. P., Belokurov V., Pettini M., Olszewski E. W., 2015, MNRAS, 448, 2687

Johnson J. A., 2019, Science, 363, 474

Johnson J. W., Weinberg D. H., 2020, MNRAS, 498, 1364

Johnson J. W., et al., 2021, arXiv e-prints, p. arXiv:2103.09838

Karakas A. I., 2010, MNRAS, 403, 1413

Karakas A. I., Lugaro M., 2016, ApJ, 825, 26

Karakas A. I., Lugaro M., Carlos M., Cseh B., Kamath D., García-Hernández D. A., 2018, MNRAS, 477, 421

Kroupa P., 2001, MNRAS, 322, 231

Limongi M., Chieffi A., 2018, ApJS, 237, 13

Mollá M., Vílchez J. M., Gavilán M., Díaz A. I., 2006, MNRAS, 372, 1069

Nomoto K., Kobayashi C., Tominaga N., 2013, ARA&A, 51, 457

Pilyugin L. S., Vílchez J. M., Thuan T. X., 2010, ApJ, 720, 1738

Schaefer A. L., Tremonti C., Belfiore F., Pace Z., Bershady M. A., Andrews B. H., Drory N., 2020, ApJ, 890, L3

Sukhbold T., Ertl T., Woosley S. E., Brown J. M., Janka H. T., 2016, ApJ, 821, 38

Ventura P., Di Criscienzo M., Carini R., D'Antona F., 2013, MNRAS, 431, 3642

Vincenzo F., Belfiore F., Maiolino R., Matteucci F., Ventura P., 2016, MNRAS, 458, 3466

Weinberg D. H., Andrews B. H., Freudenburg J., 2017, ApJ, 837, 183

Woosley S. E., Weaver T. A., 1995, ApJS, 101, 181